Korean J. Chem. Eng., 40(9), 2138-2148 (2023)
DOI: 10.1007/s11814-023-1501-4

pISSN: 0256-1115
eISSN: 1975-7220

Gas transport characteristics of mixed matrix membrane containing MIL-100 (Fe) metal-organic frameworks and PEBAX precursors

Vahid Pirouzfar*,†, Narges Roustaie*, and Chia-Hung Su,†**

*Department of Chemical Engineering, Central Tehran Branch, Islamic Azad University, Tehran, Iran
**Department of Chemical Engineering, Ming Chi University of Technology, Taiwan
(*Received 14 October 2022 • Revised 20 May 2023 • Accepted 24 May 2023*)

Abstract−This research scrutinized the effect of adding MIL-100 (Fe) metal-organic frameworks (MOFs) on the PEBAX membranes in two grades, 1657 and 2533. Initially, the intended membranes were synthesized by the solution-casting method. Then, XRD and SEM were applied to examine the influence of adding MIL-100 (Fe) to the structure of both membranes. Consequently, the separation function of the pair gases of CO_2/CH_4, CO_2/N_2, and CO_2/O_2 and their permeability were considered at the pressure of 3.5 bar and temperature of 25 °C. Eventually, their function was compared by Robeson diagrams of 1991 and 2008. According to Robeson diagrams, the comparison outcomes indicated that the PEBAX1657/MIL-100 (Fe) and PEBAX2533/MIL-100 (Fe) membranes containing 5% of MOF represent better performance in separating CO_2/CH_4. However, their function for separating the considered gases requires more modifications.

Keywords: Mixed Matrix Membrane, MOF, MIL-100, PEBAX, Selectivity

INTRODUCTION

Membrane technologies have come into wide consideration for several reasons. Membrane-based separation systems are regarded as an emerging and reliable alternative for CO_2 capture, binary- and multi-component separations, and sweetening applications [1]. This is owing to reasons such as low energy consumption, small footprint, a wide range of membranes available in the market, good thermal and mechanical stability, negligible pressure drop, high system efficiency, and low capital and operating costs compared to the typical separation methods [2,3]. On the other hand, membrane systems have inherent challenges such as plastination, low performance, and selectivity-permeability trade-offs that must be addressed to be applied on larger scales [4-6]. However, membrane-based gas separation systems have yet to be widely employed on large scales due to their incompatible membrane permeability and selectivity [7-9].

Many invaluable efforts have been made to address the challenges of membrane-based systems, mainly to develop high-efficiency and robust membranes [10-13]. The studies conducted in the previous years examined the new types of polymers as starting materials [14-16], among which copolymers like PEBAX are commercial thermoplastics, grabbed significant attention [8,17]. It was realized that PEBAX-based membranes could provide better separation performance than other alternatives, specifically when a mixture of polar and non-polar gases is fed to the system [8].

Despite the remarkable interest highlighted in the literature, many gaps and shortcomings (i.e., selectivity-permeability trade-off) should be addressed [18]. One of the previous techniques was based on incorporating nano-scale fillers to fabricate either mixed matrix membranes (MMMs) or nanocomposite membranes (NCMs). Regarding MMMs, nanofillers such as carbon molecular sieves [19], zeolites [20], MOFs [4,5], active carbon [6], and carbon nanotubes (CNTs) have been considered an impressive alternative for a long while [21,22]. However, fabricating MMMs, including the mentioned nanoparticles, was associated with their own intrinsic challenges as well. For instance, weak particle-polymer matrix interactions and non-homogeneous diffusion of the particles through the continuous polymer phase are regarded as the main barriers based on the outcomes of the related works [23,24]. MOFs offer a large specific surface area and great percentages of porosity, and the size of their nanopores can be efficiently controlled, while their dispersion within the polymer matrix can be enhanced by incorporating a wide spectrum of ligands and metals [4,5]. As a novelty, a wide spectrum of chemically modified MOFs was employed as nanofillers throughout efforts to fabricate high-performance MMMs based on PEBAX with a focus on exploiting (ZIF-8) [25] graphene oxide [26], UiO-66 [27], and MIL-53(Al) [28], MIL-101 [29] to enhance the membranes' permeability-selectivity trade-off.

MIL-100 (Fe) has drawn significant attention for many applications because of advantages such as high surface area, tunable pore sizes, highly porous structure, and remarkable adsorption capacity [30]. Moreover, MIL-100 (Fe) offers incredible permeability and selectivity. At the same time, it shows higher compatibility with polymers using the organic ligands present within the MOF structure, which leads to a better affinity to polymers [31]. In addition, the framework of this MOF includes $[Fe_3O(X)(H_2O)_2]^{6+}$ (X=OH- or F-) clusters and 1, 3, 5-benzene tricarboxylic acid (H_3BTC) anions

†To whom correspondence should be addressed.
E-mail: v.pirouzfar@iauctb.ac.ir, chsu@mail.mcut.edu.tw

with a rigid zeotype structure [23,32]. On the one hand, iron, the metal center of MIL-100 (Fe), is inexpensive, nontoxic, and environmentally friendly compared to other metals (i.e., Co, Cr, etc.) [33,34]. MIL-100 has a flexible pore structure, large specific surface area, good water stability and abundant adsorption sites as effective environmental adsorbents. With the focus on governing mechanisms in adsorption, adsorption performances, adsorption process parameters of the MIL-100, in water and gases under various conditions, it can be said that this MOF can be applied as high-performance material for gas separation and adsorption applications specially for CO_2 and CH_4 [34]. Also, for the sake of appropriate potential interacting sites and ultra microporosity, MIL-100 may be favorable for the selective adsorption of CO_2 over other gases including CH_4, N_2, H_2 and CO.

Therefore, the main innovation of the study is the excellent performance of MIL-100 (Fe) in the gas separation process. Regardless, the effect of adding MOF with an optimized and suitable structure on two selected grades from PEBAX polymer has been scrutinized in this research. Furthermore, XRD and SEM tests have been applied to assess the optimized membranes, while the effects of adding MIL-100 (Fe) to the structure of both types of polymers and their interaction have been measured as one of the innovations of this research. Finally, the features were evaluated, and the separation of the paired gases of CO_2/CH_4, CO_2/N_2, and CO_2/O_2 and their permeations were considered.

MATERIALS AND METHODS

1. Polymeric Precursors

PEBAX copolymers were used as base polymers for MMMs fabrication in this study. Table 1 displays the specifications of the PEBAX 2533 and PEBAX 1657. The whole material considered in the research has a purity of above 99.9%. Moreover, the characterizations of Dimethylformamide (DMF), which was utilized as the solvent for the membrane synthesis, are illustrated in Table 2. Pure gases of N_2 and CO_2 were employed as feed to test and assess the permeability of the membranes.

2. Synthesis of MOF (MIL-100) Fe

The Fe Lewis acid sites are produced by omitting two molecules of H_2O belonging to the octahedra Fe bases and partially removing anions through vacuum activation. Therefore, many Fe Lewis acidic sites can be obtained in pores within the MIL-100 (Fe) synthesis by considering the functions of this process. Structural studies indicate remarkable substances for surface absorption that can be utilized in processes requiring surface absorption and desorption [6].

Table 1. The properties of the PEBAX polymer grades

Properties	Unit	PEBAX1657	PEBAX2533
Contents PE	Wt.%	60	80
Density	g/cm^3	1.14	1
Melting point	°C	204	134
Glass transition	°C	−56	−65
Stress in tears	MPa	32	32

Table 2. DMF solvent properties

Name	Dimethylformamide [$(CH_3)_2NCH$]
Molecular mass	73.09 $g \cdot mol^{-1}$
Boiling point	153 °C
Melting point	60.5 °C
Density	948 $mg \cdot mL^{-1}$
Steam pressure	516 Pa
Flash point	58 °C

3. Laboratory Equipment

The magnetic stirrer includes a magnet with a cover that is neutral to all chemicals. There is also a hot plate and a magnetic engine inside the device. When the magnet inside the engine starts rotating, the magnet inside the solution container moves it. So, the magnet's temperature and rotation speed inside the solution container can be set and controlled. Fig. 1 features a schematic of a membrane module and magnetic stirrer. A prob-sonicator is a metallic container containing some water. This device was used to disperse and diffuse nanoparticles in liquids and degas the membrane solution.

A typical sonicator has a chamber on which a probe can be placed to detect the presence of a generating source. One of the main benefits of this device is the low number of moving parts and the tank. This issue will reduce the erosion and friction of the device,

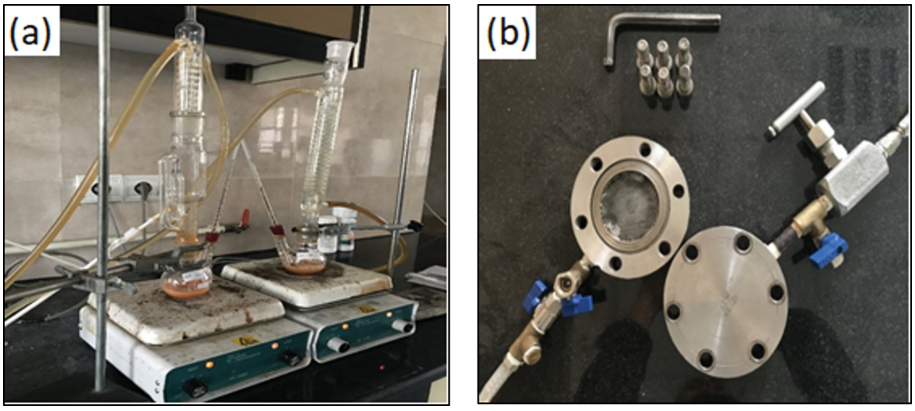

Fig. 1. The (a) membrane preparation setup and (b) membrane module.

and on the other hand, it will also increase the cleaning time of the device. To create a uniform mixture, one of the constituents must be reduced to the smallest possible particles to obtain the power of uniform diffusion in the second substance, which is usually a liquid. The chemical effects of ultrasound occur due to the effects of ultrasound waves on chemical systems. In this device, converting an electric current into a mechanical vibration causes the homogenization of the solution. This device creates strong pressure waves in a liquid environment; pressure waves cause flow in the liquid and, under suitable conditions, cause the cavitation phenomenon. When liquids are exposed to ultrasonic waves, materials will diffuse due to high and low-pressure cycling. During low-pressure cycles, small vacuum bubbles are created in the liquid. When these bubbles reach a specific size, they strongly join at high pressures. The created current will eventually lead to a strong collision of the particles and aggregate them, releasing them. The explosion of the bubbles will produce a shock wave with enough energy to break the covalent bond. The shear force resulting from bubble explosion and turbulent currents caused by acoustic vibration is used for cell homogenization and destruction.

4. MMM Preparation Procedures

The solution-casting method was used to make the membrane. Indeed, the suitable thickness in this experiment was considered to be 100 μm. For this purpose, the polymer and nanoparticle were weighed by mixing different percentages of 5, 10, and 15 wt% of nanoparticles. To diffuse the nanoparticle through the solution and have a homogeneous composite and pores with a homogeneous gap, the beaker containing the nanoparticle and solvent was put in the prob-sonicator for 20 min. The solution here was mixture of various nanoparticles prepared based on the thickness size and weight percentage. After using the prob-sonicator, if the solution is still stable for more than 5 min, the solution is considered to be dispersed. After the nanoparticle solution was added to the polymer, the flask was put on the hot plate. The thermometer and the pipe were connected to the flask, and the magnet was dropped into the flask. To completely disperse the MIL-100 and the intended polymer by rotating the magnet on the stirrer device, the stirring was performed at 110 to 120 °C for 4 hours. After several trials, it was determined that 240 min is long enough for complete dissolution and homogenization. A homogeneous solution was obtained after 225 min. In the last 15 minutes, one drop of oil was added to the solution to separate the membrane from the plate while it was being stirred. One hour earlier, the glass plate was washed with distilled water. It was put in the oven at the temperature of 70 °C.

Note that homogeneous diffusion on the plate had the same temperature when the membrane solution was poured on the plate. Later on, the composite solution, which includes PEBAX (2533 or 1657) polymer, the MIL-100 nanoparticle, and Dimethylformamide (DMF) solvent, was poured on the plate slowly, and a film with a thickness of 100 μm was obtained. The prepared films were exposed to the open air in clean conditions for one or two days to allow the solvent to evaporate completely. In the next step, the membrane was put in the oven for 3 hr at 70 °C before separating from the plate to remove the remaining solvents within the polymer structure. Finally, the membranes were removed from the plates and used for performance tests or characterizations immediately.

RESULTS AND DISCUSSION

This section details the characterization of PEBAX2533/MIL-100 (Fe) and PEBAX 1657/MIL-100 (Fe). In consequence, the function of these two membranes in the separation process of CO_2/CH_4, CO_2/N_2, and CO_2/O_2 is considered. The XRD and SEM tests were applied to analyze the membrane body's structure and surface morphology.

1. Characterization Results of Nanocomposite Membranes

1-1. XRD Test

To study the structural (crystalline-amorphous) evaluations, some characteristic tests were done on obtained PEBAX2533 and PEBAX1657/MIL-100 (Fe) nanocomposite membranes (Fig. 2). As indicated in Fig. 2(a), the PEBAX1657/MIL-100 (Fe) membranes reflected one high, broad peak and two high sharp peaks in the 23.85 and 21.45° region between angles from 15 to 25°. The wide peak reveals the amorphous structure of the PEO phase of PEBAX 1657 polymer, which has been formed in this region. The low-range long peaks are related to the crystalline phase of PA polymer [6]. Moreover, the 5.56 and 11.05° peaks disclose the presence of MOF in the membrane structure. Their intensity is diminished because of diffusion in the polymer environment. As the amount in the polymer structure is increased to 0.15%, a slightly intensive peak has been shown [7,17]. Fig. 2(b) illustrates the results of XRD for the PEBAX 2533/MIL-100 (Fe) for the nanocomposite membrane. These membranes include an amorphous and crystalline phase in one wide peak (15 to 25°) and two high sharp peaks (23.85 and 21.69°), respectively. Notably, the wide peak reveals the amorphous structure of the PTMO phase of PEBAX2533 polymer in this region. High sharp peaks are related to the crystalline phase of PA polymer [7,17]. Similarly, the peaks 5.56 and 11.05° indicate the presence of MOF in the membrane structure. Because all the nanocomposite membranes made in this research were synthesized by applying the DMF [7], the boiling point of this solvent is high; it ends up producing membranes with mostly crystalline structures [8]. Thus, the presence of crystalline phases in membrane structure could be predicted. Besides the crystalline polymer structure, it is significant to remark on the situation of crystalline peaks and determine the permeation properties in membranes. According to the Bragg equation ($n\lambda=2d\sin\theta$), when the amounts of 2θ are decreased, the d-spacing increases. The d-spacing is a criterion to measure the molecular spacing of inter-polymeric chain. As the d-spacing increases, there is more tendency to transmit gas molecules [6,18]. The d-spacing for grade 2433 will be more than 1657 due to different peaks of PEBAX. Note that the fabrication of membranes using DMF as a solvent would lead to the formation of a semi-crystalline structure since that can be related to the higher boiling point (and consequently lower evaporation rates) of DMF (153.2 °C) compared to that of the solvents such as H_2O+EtOH blend (75 °C) [18].

1-2. SEM Results

In addition, the SEM test was applied to examine the effect of adding MIL-100 (Fe) to PEBAX2533 and PEBAX1657 on the nanocomposite membranes' structure and surface. Fig. 3 shows the results of this experiment. As observed, using PEBAX 2533 polymer can produce more porous membranes, and the presentation

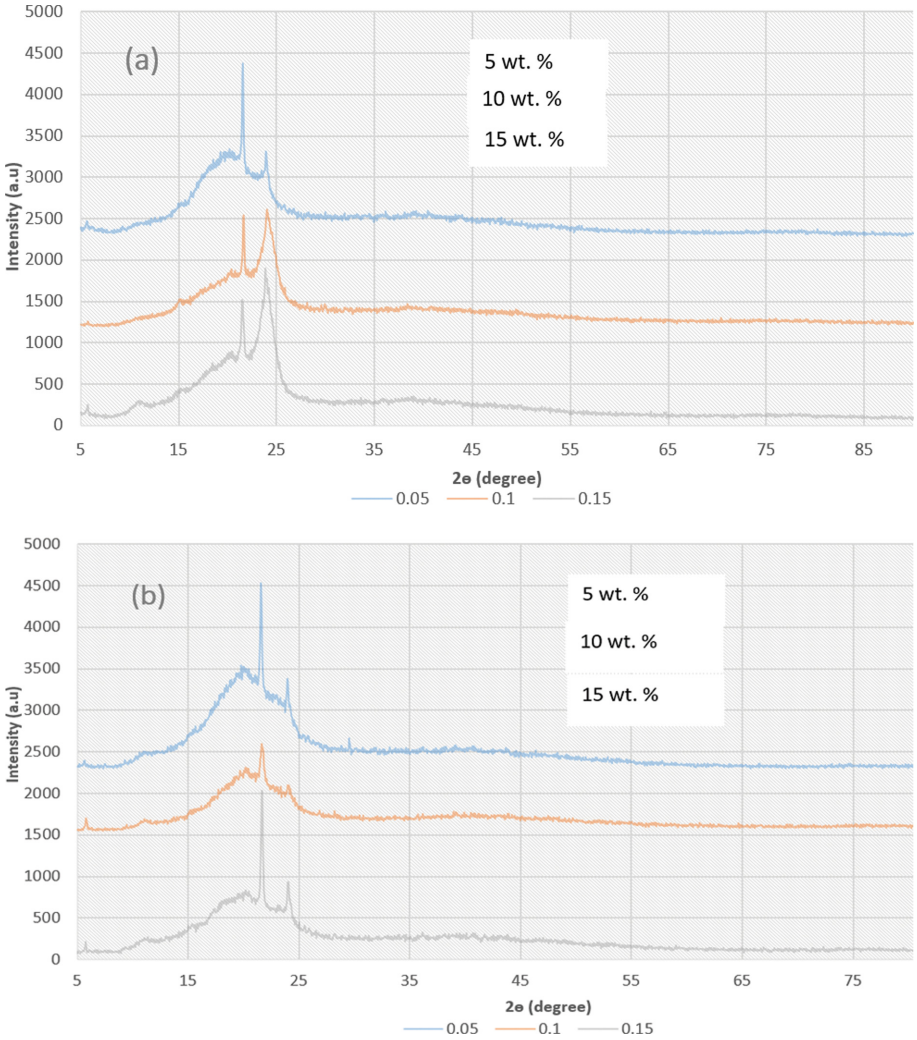

Fig. 2. X-ray diffraction test results for (a) PEBAX1657/MIL-100 (Fe) and (b) PEBAX2533/MIL-100 (Fe) membranes with various loading percentage.

makes this of TMO monomers [9]. Clearly, poly tetra methylene is identified as a part of the PEBAX2533. Also, this factor makes synthesized membranes have a more porous level, while poly ether amide polymer, which is in the structure of PEBAX1657, is directed into making bigger pores and a more porous structure [10]. This is caused by more effortless movement and more flexibility of PEBAX polymeric chains on the surface [11].

As pointed out, PEBAX is an elastomer thermoplastic, which is a compound of linear chains of hard polyamide (PA) such as nylon-6 (6PA-) and nylon-12 (12PA-). It is set beside the poly ether monomers (PE) and provides flexibility and mechanical power in the final polymer. In addition, poly tetra methyl oxide (PTMEO), which presents excellent properties for gas separation, has been added to the structures of PEBAX2533. According to the results of SEM, it is concluded that the presence of poly tetra methyl oxide (PTMEO) increases the intervals of d, which enhances gaseous permeation.

Overall, it demonstrates that the synthesized membranes hold a less dense and suitable structure. As indicated, the effect of adding MIL-100 (Fe) to PEBAX1657 and 2533 polymers on the structure of synthesized membranes has been shown. Observing the SEM images can pave the way to realize that the MOF amount leads to more roughness on the membrane surface. Finally, it improves the absorption process and gas dissolution [14]. Furthermore, it is observed that the lumping amount is increased as this substance is enhanced. Eventually, it might bring about non-selective masses on the surface and the membrane structure [11,35]. Several characterization techniques can be considered in future works. For example, time-of-flight secondary ion mass spectrometry (ToF-SIMS), focused ion beam (FIB), and atomic force microscopy (AFM) can lead to acceptable results.

2. Separation Performance of Nanocomposite Membranes

The gaseous separation efficiency of the PEBAX1657 and 2533 -based membranes was examined after adding MIL-100 (Fe) under a pressure gradient of 3.5 bar at 25 °C. In this research, the permeability of CO_2, CH_4, N_2, and O_2 gases, as well as their corresponding pair gas selectivity (CO_2/CH_4, CO_2/N_2, and CO_2/O_2), were evaluated (Fig. 4). As displayed in Fig. 4(a), the CO_2 permeability across the membranes synthesized based on PEBAX2533 are

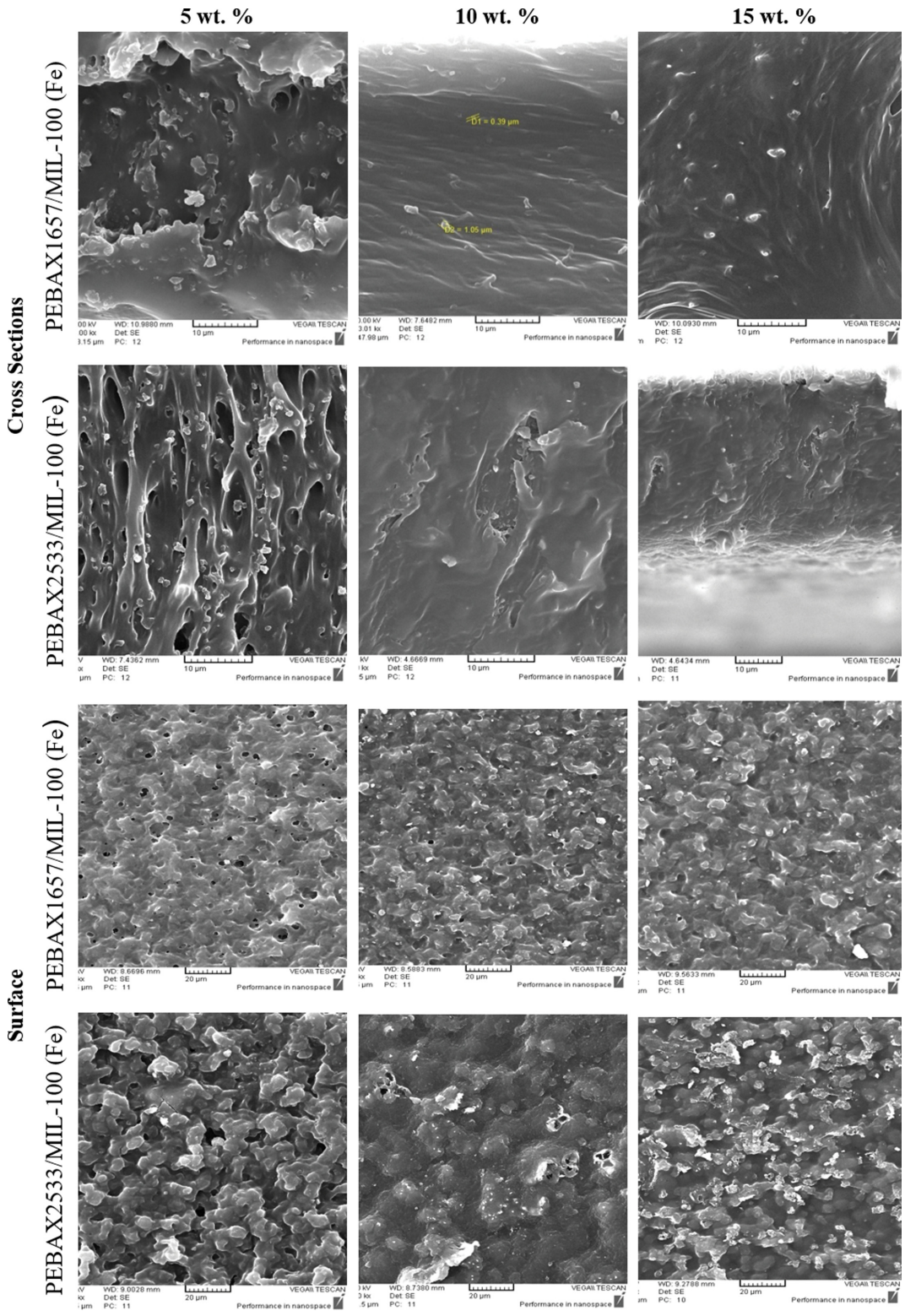

Fig. 3. SEM photographs of the surface and cross sections of the PEBAX1657/MIL-100 (Fe) and PEBAX2533/MIL-100 (Fe) nanocomposite membranes in various loading percentage.

more than those synthesized with PEBAX1657. Such an increase is caused by the presence of poly tetra methyl oxide monomers that form more porous and flexible membranes [36]. Thus, the polymeric tetramethylene oxide (PTMEO) segment, the flexible polyether segment of PEBAX 2533, facilitates the transition of gaseous molecules [36]. Moreover, since the CO_2 affinity to PTMEO

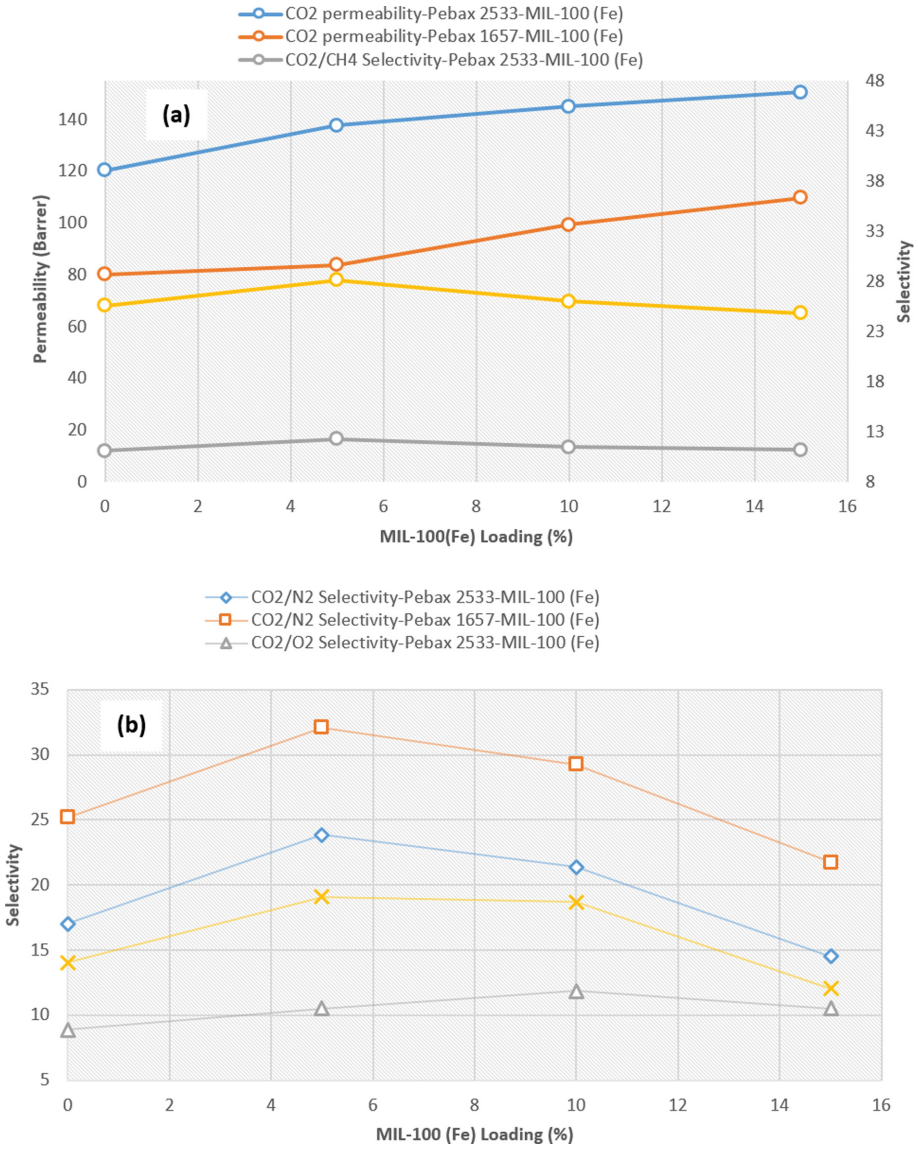

Fig. 4. Comparison of the separation performance of PEBAX1657/MIL-100 (Fe) and PEBAX2533/MIL-100 (Fe) membranes due to increasing MIL-100 (Fe) loading percentages; (a) CO_2 permeability and (b) gas pair selectivity of CO_2/N_2 and CO_2/O_2 at pressure of 3.5 bar.

is significantly higher than PE owing to the creation of hydrogen bonds, such affinity is high in N_2, methane, and oxygen. As indicated in the XRD analysis, PEBAX 2533 is more amorphous than PEBAX 1657, leading to an increase in the d-spacing and an enlargement in the membrane pores, allowing more gas molecules to pass through the membrane. However, the solution-diffusion mechanism is identified as the dominant mechanism explaining the gas permeation through the dense membranes; notably, it is true for methane gas as it is for CO_2 [15].

As shown in Fig. 5, PEBAX 2533-based membranes show less selectivity than those made with PEBAX1657. It is indicated that the permeation amount of CO_2 increased in both membranes after MIL-100 (Fe) addition to the polymer matrix. This is related to the free fraction volume (FFV) developed due to the formation of pores around MOF-diffused nanoparticles [37]. Moreover, the affinity to polar gases like CO_2 was increased in synthesized membranes when MIL-100 (Fe) was added to PEBAX matrix because of OH polar functional agents' formation [38]. The FFV enhancement and the increase of OH groups are responsible for the steady permeation increase of CO_2 [1].

The SEM images show that the increase of MOF amount directs into lumping more nanoparticles. At last, more non-selective surfaces and sections are made on the structure of the membranes. As observed, this factor affects the total selectivity of the membrane and its operation. Accordingly, a reduction in permeation of CH_4, N_2, and O_2 molecules was witnessed owing to the higher crystallinity of the PEBAX1657 polymer compared to PEBAX2533 as well as the formation of denser structures leading to a reduction in the permeation of the mentioned molecules [1,18,28]. For this reason, better selectivity values in PEBAX1657/MIL-100 (Fe) membranes were observed compared to PEBAX2533/MIL-100 (Fe). Fig. 5 reveals that the selectivity of the pair gas of CO_2/N_2 is

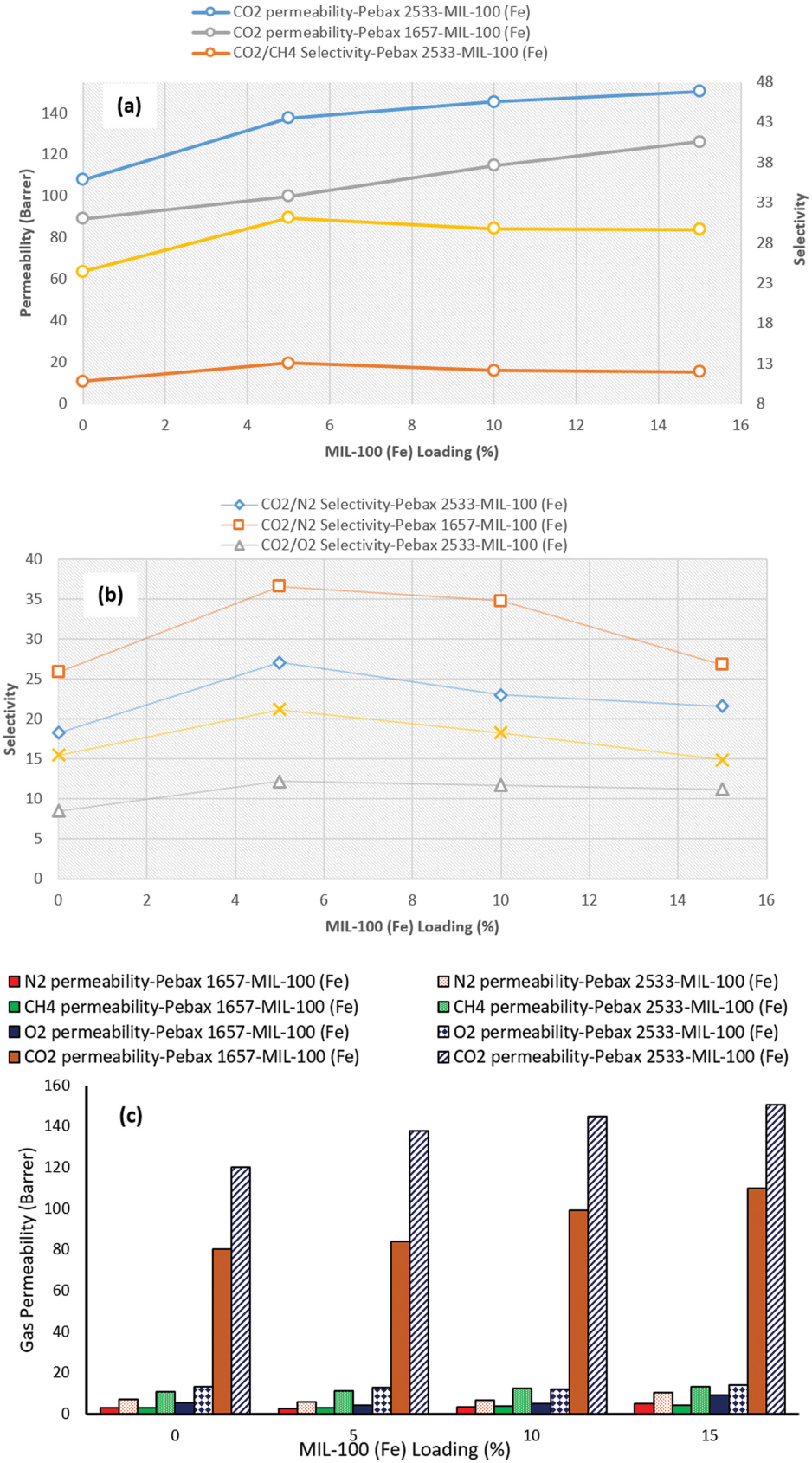

Fig. 5. Comparison of the separation performance of PEBAX1657/MIL-100 (Fe) and PEBAX2533/MIL-100 (Fe) membranes due to increasing loading percentages of MIL-100 (Fe); (a) CO_2 permeability and CO_2/CH_4 selectivity at pressure of 5.5 bar (b) selectivity of CO_2/N_2 and CO_2/O_2 at pressure of 5.5 bar. (c) Permeability of CO_2, CH_4, N_2 and O_2 at a pressure of 3.5 bar.

greater than that of CO_2/O_2 and CO_2/CH_4. Evidently, it is inferred that the least amount of gaseous permeation is related to N_2 gas, methane gas, and carbon dioxide, correspondingly.

As outlined, the solution-diffusion mechanism is the dominant mechanism for passing gases through dense membranes such as gaseous ones. Based on this theory, the gaseous molecules permeate the membrane and pass through it because they tend to the membrane surface (determining the dissolution coefficients) and are condensed by the critical temperature [14]. Accordingly, the molecular polar bond among the gases considerably influences the surface dissolution stage. In fact, the carbon dioxide molecules will have the highest condensation while in touch with the polymeric structure of the membrane. As a result, it leads to more permeation than other gases tested in this research [11].

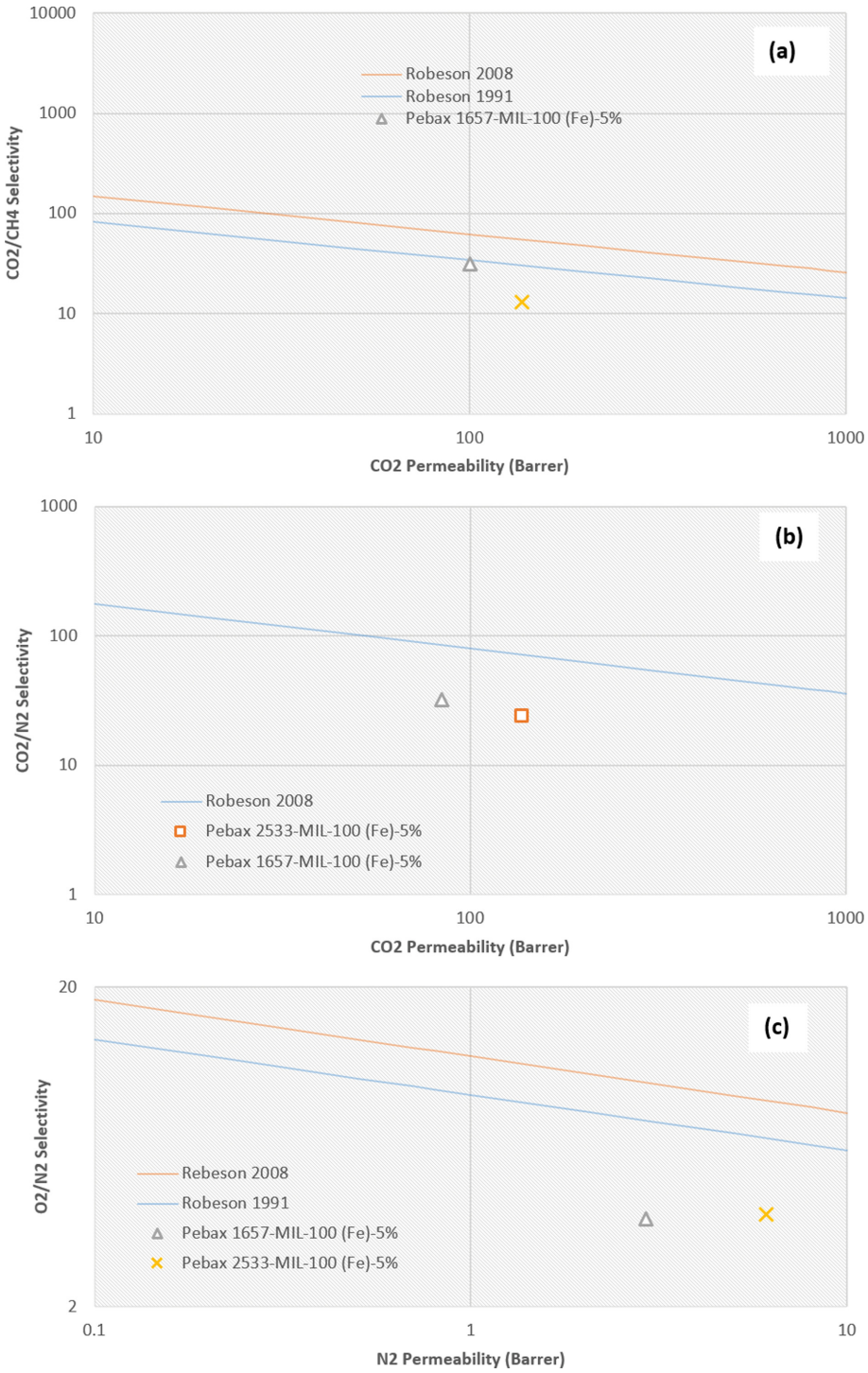

Fig. 6. Separation data of the PEBAX1657/MIL-100 (Fe)- 5% and PEBAX2533/MIL-100 (Fe)- 5% membranes compared to the 1991 and 2008 Robson diagrams for (a) CO_2/CH_4 vs CO_2 permeability; (b) CO_2/N_2 vs CO_2 permeability; and (c) O_2/N_2 vs N_2 permeability.

The permeability of PEBAX/MIL-100 (Fe) was improved considering the mixed effects of permeation-dissolution and the molecular screening mechanism. The outcomes cannot be explained only by one of the mechanisms. However, the addition of MOF can make a remarkable change in the permeation of carbon dioxide as it is attributed to the ideal selectivity of CO_2/N_2, CO_2/CH_4, and CO_2/O_2 pair gases. Notably, carbon dioxide passes through MIL-100 (Fe) pores, which can remarkably prevent the permeation of bigger molecules in the MOF pores and the permeation of CO_2 changes [39-41]. From another point of view, although methane gas is a non-polar molecule, it has polar bonds tending these molecules to the fine PEBAX polymer segments resulting in higher permeations compared to O_2 and N_2 [36]. The next influential factor is the gases' kinetic diameter, which determines their amount and permeation coefficient. Since the kinetic diameter of carbon dioxide (3.3 A) is less than methane (3.8 A), N_2 (3.64 A), and oxygen (3.46 A), it will have a higher permeation coefficient. Likewise, O_2 and N_2 molecules are non-polar with non-polar bonds.

Nonetheless, oxygen has a smaller kinetic diameter and reflects more dissolution in the membrane by making hydrogen bonds with OH groups in the membrane structure and MOF [8,39,42]. Fig. 5(c) illustrates the permeation results of different gases from the PEBAX1657MIL-100 (Fe) and PEBAX2533/MIL-100 (Fe). As observed, CO_2 has scored more permeability in all parentages. The permeations are as below:

$$CO_2>O_2>CH_4>N_2$$

The rubber nature of PEBAX makes the more polar nature of CO_2 more permeable than other gases. On the other hand, the kinetic diameter of CO_2 is smaller than O_2, N_2, and CH_4. It may be directed into more permeation of this gas in comparison with other gases [6,39]. Moreover, the weak solubility of N_2 may be caused by the low permeability of the more kinetic diameter. Finally, it leads to less permeation. The permeation-dissolution mechanism has been widely accepted in order to explain the permeation of gases through the polymeric membrane. It is noteworthy that the principle of this mechanism is based on the gas transition through MIL-100 (Fe) caused by the simultaneous impact of the factors of MOF percentage compound, the size, and structure of pores. MIL-100 has suitable molecular screening effects for the sake of engineered crystalline structures and the size of pores. In fact, the permeability of gases is enhanced by adding MIL-100 (Fe) to the structure of both PEBAX grades [43,44].

Fig. 6 discloses the effect of adding different percentages of MOF to the PEBAX structure on the separation operation of the synthesized membranes at a pressure of 5.5 bar. Fig. 6(a) indicates that the permeation of carbon dioxide has been increased for both membranes with the PEBAX base as the MOF amount enhanced at the pressure of 5.5 bar. Besides, it is observed that the trend of changes at the pressure of 5.45 bar is similar to the tests done at the pressure of 3.5 bar. However, both permeability and selectivity have been enhanced to higher amounts. So, as the pressure is increased from 3.5 to 5.5 bar, the PEBAX1657/MIL-100 (Fe) membrane has reflected better operation than PEBAX2533/MIL-100 (Fe) in the separation of the tested gases. This phenomenon is caused by higher FFV of PEBAX2533/MIL-100 (Fe) membranes which are dense by pressure increase. As a result, the gas permeation coefficient is reduced in polymer due to the (D=Aexp($-\gamma v^*$/FFV) Cohen-Turnbull)).

It is observed that the highest separation amount and ideal selectivity were observed in membranes with a loading percentage of 5 MOF. This phenomenon is brought about by MIL-100 (Fe) lumping in the mixed matrix membrane [39].

3. Comparison of the Permeability and Selectivity Results of Prepared MMM

The graphs of 1991 [38] and 2008 [45] were used to scrutinize the separation operation of the synthesized membranes with other mixed matrix membranes and nanocomposite. These graphs have been achieved based on the selectivity and permeability data of a certain number of gases in previous studies designed by Robeson. Much research on gaseous membrane separation has considered these graphs an operational criterion. In fact, if the operation of a membrane touches the graph or passes through it, its operation is acceptable [7,39]. The graphs of Fig. 6 indicate that the PEBAX1657/MIL-100 (Fe) membrane operation on the Robeson graph of 1991 is associated with CO_2/CH_4 separation, and PEBAX2533/MIL-100 (Fe) has touched it. The function of the synthesized membranes is lower than the Robeson graphs of 1991 and 2008 in separating the CO_2/N_2 and O_2/N_2 pair gases. The PEBAX1657/MIL-100 (Fe) membrane has a relatively suitable operation to separate methane and carbon dioxide gases. The gradual increase of permeation by pressure enhancement is attributed to increasing the absorption of CO_2 in the polymeric membrane [44].

According to the given explanations, the performance of CO_2 can be improved by tuning the pressure based on the hydrogen bonds among oxygen atoms existing in CO_2 and Amide operational groups in PEBAX. In fact, the permeation of CO_2 in PEBAX2533-MIL-100 (Fe) is improved more than in PEBAX1657-MIL-100 (Fe) (Fig. 6(c)). Additionally, more carbon dioxide permeation might be related to enhancing the permeability of CO_2 in the mixed matrix membranes compared with other gases. The main reason is that since OH bonds are in the MIL-100 (Fe) structure, CO_2 tends to pass through the MOF pores more than other gases. In order to highlight the superiority of the proposed method over the previous ones, Table 3 compares the performances of the Pebax 2533 MIL-100 (Fe) membranes fabricated in the current study with some related works. Due to the results, the MIL-100 (Fe) incorporated samples of the current study provided an acceptable separation performance.

4. Economical Justifications

In terms of economy, one of the basic processes in many chemical engineering operations is gas separation. With the industry's demand to lower energy requirements and operating costs and the need to increase separation efficiency, many studies have been conducted to improve the process. In the last two decades, gas separation using polymer membranes has drawn much attention for its advantages, such as low energy cost and selectivity capabilities. One of the materials successfully used in gas separation is poly (ether block amide) copolymers, often referred to as Pebax. With its high selectivity for polar/non-polar systems (e.g., CO_2/H_2, H_2S/CH_4, or CO_2/N_2) and permeability behavior similar to a rubbery polymer, Pebax is an interesting choice as a membrane material in many membrane separation applications.

Table 3. Comparison of different MOF-based membranes performance

Base polymer	MOF type	Filler loading (%)	Pair gases	Condition		Performance		Reference
				Pressure (bar)	Temperature (°C)	CO_2 permeation (Barrer)	Ideal selectivity	Current study
Pebax2533	MIL-100 (Fe)	5	CO_2-N_2	5.5	20	137.7	23.8	Current study
Pebax2533	MIL-100 (Fe)	5	CO_2-O_2	5.5	20	137.7	12.2	Current study
Pebax2533	MIL-100 (Fe)	5	CO_2-CH_4	5.5	20	137.7	12.3	Current study
Pebax1657	MIL-100 (Fe)	10	CO_2-N_2	5.5	20	83.9	32.1	Current study
Pebax1657	MIL-100 (Fe)	10	CO_2-O_2	5.5	20	83.9	19.1	Current study
Pebax1657	MIL-100 (Fe)	10	CO_2-CH_4	5.5	20	83.9	28.6	Current study
Pebax1657	UiO-66-NH_2	10	CO_2-O_2	3	20	97.5	18.1	[46]
Pebax1657	UiO-66-NH_2	10	CO_2-N_2	3	20	118.3	56.6	[46]
Pebax1657	UiO-66	10	CO_2-O_2	3	20	97.5	18.1	[46]
Pebax1657	UiO-66-NH_2	10	CO_2-O_2	3	20	118.3	19.2	[46]
Pebax1657	ZIF-8	16	CO_2-CH_4	8	60	758	16.10	[41]
Pebax1657	UiO-66 (non-honeycomb structured)	10	CO_2-N_2	3	25	130	72	[47]
Pebax1657	CuBTC	20	CO_2-CH_4	3	30	56.20	23.4	[48]
Pebax2533	ZIF-11	70	CO_2-CH_4	2	20	402.89	12.49	[49]
Polysulfone	ZIF-8	16	CO_2-CH_4	8	60	12.1	19.80	[50]
Polysulfone	$Mn(HCOO)_2$	10	CO_2-CH_4	10	60	6.83	9.16	[51]
Polysulfone	$Cu_3(BTC)_2$	10	CO_2-CH_4	10	60	304.4	3.60	[51]
Polysulfone	MIL-101	19	CO_2-CH_4	10	20	32.0	23.50	[52]
Pebax1657	MIL-53(Al)	10	CO_2-CH_4	35	10	129	23.3	[53]
Pebax1657	NH2-MIL-53(Al)	10	CO_2-CH_4	35	10	149	20.5	[53]
Pebax®1657	NH2-MIL-53(Al)	10	CO_2-H_2	35	10	149	10.6	[53]

CONCLUSIONS

Both types of membranes based on PEBAX with different grades and loading percentages of MOF were dissected and observed with the contribution of the XRD experiment of the amorphous (polyamide) and crystalline phases (poly ether oxide and poly tetra ethylene oxide). Moreover, two sharp peaks at 5.56 and 11.05° proved the presence of MOF. According to the SEM results, it was observed that membranes synthesized based on the PEBAX2533 held a more porous structure in comparison with the ones synthesized based on PEBAX1657. Adding MIL-100 (Fe) to PEBAX creates more roughness on the membrane surface. Additionally, as this MOF was increased, the lumping amount was enhanced. Eventually, it brings about non-selective masses on the surface and membrane structure. The outcomes of permeability and selectivity experiments demonstrated that carbon dioxide has the highest permeability, whereas N_2 gas revealed the least permeability through the synthesized membranes for the sake of more chemical tendency to the membrane surface and the small kinetic diameter. The permeability of methane gas was more than oxygen gas. Moreover, the synthesized membranes based on PEBAX2533 revealed more permeability, whereas membranes containing PEBAX1657 reflected better selectivity. Adding MIL-100 (Fe) to the membrane structure caused to improve the separation and permeation of all the intended gases. At the same time, the enhancement of this substance decreased the selectivity of the paired gases despite the permeability increase. This is concluded by lumping MOFs on the surface and the structure of the synthesized membranes. As the operating pressure was increased to 5.5 bar, improvement of the separation operation was observed in all data. The results compared with Robeson diagrams indicated that PEBAX1657/MIL-100 (Fe) and PEBAX2533/MIL-100 (Fe) membranes contain 5 wt% of MOF; it has a convenient operation in separating methane gas from carbon dioxide for the sake of the Robeson graph of 1991. However, as mentioned, their operation needs more modifications to separate other gases.

Funding: The authors declare that there is no funding.

Conflict of interest: The authors declare no conflict of interest.

Data Availability: All data generated or analyzed during this study are included in this published article (and its supplementary information files).

REFERENCES

1. H. R. Mahdavi, N. Azizi and T. Mohammadi, *J. Polym. Res.*, **24**(5), 1 (2017).
2. Y. Ban, M. Zhao and W. Yang, *Front. Chem. Sci. Eng.*, **14**(2), 188 (2020).

3. X. Liu, *Front. Chem. Sci. Eng.*, **14**(2), 216 (2020).
4. N. Behnia and V. Pirouzfar, *Polym. Bull.*, **75**(10), 4341 (2018).
5. S. M. Hosseini, V. Pirouzfar and H. Azami, *J. Membr. Biol.*, **250**(6), 651 (2017).
6. V. Pirouzfar, *High performance gas separation carbon molecular sieve membranes*, LAP LAMBERT Academic Publishing (2015).
7. M. Yarmohammadi, A. K. Adeli, M. Z. Pedram, M. Shahidzadeh and V. Pirouzfar, *J. Appl. Polym. Sci.*, **135**(45), 46707 (2018).
8. M. Salimi and V. Pirouzfar, *J. Aust. Ceram. Soc.*, **54**(2), 271 (2018).
9. V. Pirouzfar, A. Zarringhalam Moghaddam and B. Mirza, *J. Energy Resour. Technol.*, **134**(4), 041101 (2012).
10. N. Sohrabi, A. Alihosseini, V. Pirouzfar and M. Z. Pedram, *Membranes*, **10**(10), 283 (2020).
11. S. F. Soleymanipour, A. H. S. Dehaghani, V. Pirouzfar and A. Alihosseini, *J. Appl. Polym. Sci.*, **133**(34) (2016).
12. M. Sheikhi, L. Mirshekar, B. Kamarehie, M. Ghaderpoori, B. Ramavandi, F. Amini, N. Fadaie and S. Sahebi, *Chem. Eng. Technol.*, **44**(7), 1251 (2021).
13. S. Seraj, M. Sheikhi, T. Mohammadi and M. A. Tofighy, *Oil-Water Mixtures and Emulsions, Volume 1: Membrane Materials for Separation and Treatment*, Chapter 8, 305 (2022).
14. A. H. Saeedi Dehaghani, V. Pirouzfar and A. Alihosseini, *Polym. Bull.*, **77**(12), 6467 (2020).
15. N. N. Li, A. G. Fane, W. S. W. Ho and T. Matsuura, *Advanced membrane technology and applications*, John Wiley & Sons (2011).
16. R. S. Murali, S. Sridhar, T. Sankarshana and Y. V. L. Ravikumar, *Ind. Eng. Chem. Res.*, **49**(14), 6530 (2010).
17. S. Heydari and V. Pirouzfar, *RSC Adv.*, **6**(17), 14149 (2016).
18. M. Isanejad, N. Azizi and T. Mohammadi, *J. Appl. Polym. Sci.*, **134**(9) (2017).
19. C. Gu, Y. Liu, W. Wang, J. Liu and J. Hu, *Front. Chem. Eng.*, **15**, 437 (2021).
20. V. Pirouzfar and M. R. Omidkhah, *Iran. Polym. J.*, **25**(3), 203 (2016).
21. V. Nafisi and M. B. Hagg, *J. Membr. Sci.*, **459**, 244 (2014).
22. G. E. Cmarik, M. Kim, S. M. Cohen and K. S. Walton, *Langmuir*, **28**(44), 15606 (2012).
23. P. Horcajada, S. Surblé, C. Serre, D. Y. Hong, Y. K. Seo, J. S. Chang and G. Férey, *Chem. Commun.*, (27), 2820 (2007).
24. G. Dong, J. Hou, J. Wang, Y. Zhang, V. Chen and J. Liu, *J. Membr. Sci.*, **520**, 860 (2016).
25. L. Xu, L. Xiang, C. Wang, J. Yu, L. Zhang and Y. Pan, *Chin. J. Chem. Eng.*, **25**(7), 882 (2017).
26. L. Dong, M. Chen, J. Li, D. Shi, W. Dong, X. Li and Y. Bai, *J. Membr. Sci.*, **520**, 801 (2016).
27. J. Shen, G. Liu, K. Huang, Q. Li, K. Guan, Y. Li and Y. W. Jin, *J. Membr. Sci.*, **513**, 155 (2016).
28. S. Meshkat, S. Kaliaguine and D. Rodrigue, *Sep. Purif. Technol.*, **200**, 177 (2018).
29. M. A. Rodrigues, J. de Souza Ribeiro, E. de S. Costa, J. L. D. Miranda and H. C. Ferraz, *Sep. Purif. Technol.*, **192**, 491 (2018).
30. G. Gao, Y. Xing, T. Liu, J. Wang and X. Hou, *Microchem. J.*, **146**, 126 (2019).
31. Y. Fang, J. Wen, G. Zeng, F. Jia, S. Zhang, Z. Peng and H. Zhang, *Chem. Eng. J.*, **337**, 532 (2018).
32. I. Bezverkhyy, G. Weber and J. P. Bellat, *Micropor. Mesopor. Mater.*, **219**, 117 (2016).
33. F. Zhang, J. Shi, Y. Jin, Y. Fu, Y. Zhong and W. Zhu, *Chem. Eng. J.*, **259**, 183 (2015).
34. G. Chen, X. Leng, J. Luo, L. You, C. Qu, X. Dong and J. Ni, *Molecules*, **24**(7), 1211 (2019).
35. A. H. Saeedi Dehaghani and V. Pirouzfar, *Chem. Eng. Technol.*, **40**(9), 1693 (2017).
36. V. Pirouzfar, S. N. Moghaddam, S. A. H. S. Mousavi, A. H. S. Dehaghani, H. Mollabagher and C. H. Su, *J. Contam. Hydrol.*, **249**, 104048 (2022).
37. E. Schindler and F. Maier, *Manufacture of porous carbon membranes*, Google Patents (1990).
38. L. M. Robeson, *J. Membr. Sci.*, **62**(2), 165 (1991).
39. D. Q. Vu, W. J. Koros and S. J. Miller, *J. Membr. Sci.*, **211**(2), 311 (2003).
40. Y. Fang, Z. Yang, H. Li and X. Liu, *Environ. Sci. Pollut. Res.*, **27**, 4703 (2020).
41. A. Jomekian, R. M. Behbahani, T. Mohammadi and A. Kargari, *J. Nat. Gas Sci. Eng.*, **31**, 562 (2016).
42. J. Zhao, K. Xie, L. Liu, M. Liu, W. Qiu and P. A. Webley, *J. Membr. Sci.*, **583**, 23 (2019).
43. Y. Y. Fu, C. X. Yang and X. P. Yan, *J. Chromatogr. A*, **1274**, 137 (2013).
44. X.Wang, Q. Wang, F. Gao, Y. Yang and H. Guo, *ACS Appl. Mater. Interfaces*, **6**(14), 11573 (2014).
45. H. T. Lu, W. Li, E. S. Miandoab, S. Kanehashi and G. Hu, *Front. Chem. Sci. Eng.*, **15**, 464 (2021).
46. R. Sarmadi, M. Salimi and V. Pirouzfar, *Environ. Sci. Pollut. Res.*, **27**(32), 40618 (2020).
47. J. Shen, G. Liu, K. Huang, Q. Li, K. Guan, Y. Li and W. Jin, *J. Membr. Sci.*, **513**, 155 (2016).
48. T. Khosravi and M. Omidkhah, *J. Energy Chem.*, **26**(3), 530 (2017).
49. A. Ehsani and M. Pakizeh, *J. Taiwan Inst. Chem. Eng.*, **66**, 414 (2016).
50. B. Zornoza, B. Seoane, J. M. Zamaro, C. Téllez and J. Coronas, *Chem. Phys. Chem.*, **12**(15), 2781 (2011).
51. A. Car, C. Stropnik and K. V. Peinemann, *Desalination*, **200**, 424 (2006).
52. H. B. T. Jeazet, T. Koschine, C. Staudt, K. Raetzke and C. Janiak, *Membranes*, **3**(4), 331 (2013).
53. S. Meshkat, S. Kaliaguine and D. Rodrigue, *Sep. Purif. Technol.*, **200**, 177 (2018).